

Few-Shot Multi-Human Neural Rendering Using Geometry Constraints

Qian Li¹, Victoria Fernández Abrevaya², Franck Multon¹, Adnane Boukhayma¹

¹Inria, University Rennes, IRISA, CNRS, France

²Max Planck Institute for Intelligent Systems, Germany

Abstract

We present a method for recovering the shape and radiance of a scene consisting of multiple people given solely a few images. Multi-human scenes are complex due to additional occlusion and clutter. For single-human settings, existing approaches using implicit neural representations have achieved impressive results that deliver accurate geometry and appearance. However, it remains challenging to extend these methods for estimating multiple humans from sparse views. We propose a neural implicit reconstruction method that addresses the inherent challenges of this task through the following contributions: First, we propose to use geometry constraints by exploiting pre-computed meshes using a human body model (SMPL). Specifically, we regularize the signed distances using the SMPL mesh and leverage bounding boxes for improved rendering. Second, we propose a ray regularization scheme to minimize rendering inconsistencies, and a saturation regularization for robust optimization in variable illumination. Extensive experiments on both real and synthetic datasets demonstrate the benefits of our approach and show state-of-the-art performance against existing neural reconstruction methods.

1. Introduction

Human reconstruction from single images [15, 41, 53], multiple images [16, 26], RGB videos [2, 45] or RGB-D data [104, 106] has received a lot of attention, much less explored is the task of *multiple* human scenario, which is essential for scene understanding, behavior modeling, collaborative augmented reality, and sports analysis. The multi-human setting introduces additional challenges, as there is now a higher level of occlusion and clutter which hinders matching and reconstruction. Although in principle one could approach this by first detecting and then independently processing each person, simultaneous reconstruction of multiple humans can help to globally reason about occlusion at the level of the scene [38, 84], and can potentially recover coherent 3D spatial relations among the people.

Several recent works have attempted to recover multi-

ple humans from a single view [14, 22, 38, 61, 83, 84, 87, 108, 109, 111]. However, the majority of these are based on regressing the parameters of a human body model –typically SMPL [57]– which provides coarse reconstructions that lack hair, clothing, and geometric details. Multi-view settings can help resolve some of the occlusions as well as depth ambiguities, but require a dense array of RGB cameras to achieve a detailed reconstruction [16, 39, 89]. A more convenient capture system is the *sparse* multi-view setting, where only a handful of cameras is required. However, due to the decreased number of views and increased level of occlusion, existing methods require segmentation masks and a pre-scanned template mesh [55, 96], rely on a coarse body model [30, 115], or require temporal information [30, 116].

A parallel line of work simultaneously tackles the novel-view-synthesis and geometry-reconstruction problems by combining neural coordinate-based representations, *e.g.* implicit signed distance functions (SDFs) [71], with differentiable rendering [59, 90, 100, 101]. This approach has the advantage of producing, along with geometry, renderings from novel viewpoints that can capture complex surface/light interactions, increasing the scope of applications. NeRF [59], for example, uses volumetric rendering to produce impressive images under novel views, albeit at the cost of sub-optimal geometries due to the unconstrained volumetric representation. SDF-based methods [90, 100, 101], while delivering images of slightly lower quality, have been shown to produce 3D surfaces that are competitive with classical approaches. For humans, this has been leveraged to obtain geometry and appearance from monocular video [12, 37], RGB-D video [19], and sparse multi-view video [46, 52, 73, 76, 91, 93, 99, 116]. However, none of these works, with the exception of [110, 116], were designed to handle the increased geometric complexity and occlusion of the multi-human case. Current works [110, 116] address the multi-human setting, but both require a set of videos, which effectively becomes a dense array of views as long as deformations are modeled correctly.

In this paper, we address the problem of multiple 3D human surfaces and volume rendering from sparse static

multi-view images. Our key insight is that human-specific geometric constraints can be leveraged to tackle the challenging sparse-view setting.

Specifically, we first obtain a SMPL body model from the input data and use it to initialize the implicit SDF network, where we define the surface of a multi-human scene as the zero-level set of the SDF. Then, the geometry network is optimized with multi-view images by leveraging surface and volume rendering [90] along with uncertainty estimation methods [18, 77], where the SMPL meshes are treated as noisy estimations. To achieve higher rendering quality from sparse training views, we additionally propose a patch-based regularization loss that guarantees consistency across different rays and a saturation regularization that ensures consistency for variable image illuminations within the same scene.

We evaluate our method quantitatively and qualitatively on real multi-human (CMU Panoptic [40, 81]) and synthetic (MultiHuman [116]) datasets. We demonstrate results on 5, 10, 15 and 20 training views, where we achieve state-of-the-art performance in terms of surface reconstruction and novel view quality.

2. Related Work

Single-Human Reconstruction. There is a vast amount of work on reconstructing 3D humans from single images [7, 15, 41, 53, 60], monocular video [3, 45, 107], RGB-D data [9, 104, 106] and multi-view data [16, 26, 33, 82]. We concentrate here on the multi-view setting. High-end multi-view capture systems can achieve reconstructions of outstanding quality [16, 21, 26, 40, 47, 89], but require a complex studio setup that is expensive to build and not easily accessible. To alleviate this, numerous works have been proposed that use instead a sparse set of RGB cameras (*e.g.* between 2 and 15), where the lack of views and presence of wide baselines is compensated by tracking a pre-scanned template [10, 17, 23, 88, 97], using a parametric body model [6, 32], or more recently, by the use of deep learning [33, 46, 50, 52, 73, 76, 91, 93, 99].

Multi-Human Reconstruction. In contrast, there has been a limited number of works that address the problem of *multiple* human reconstruction. This is a difficult task since the presence of several people increases the geometric complexity of the scene, introduces occlusions, and amplifies ambiguities such that commonly used features like color, edges, or key points cannot be correctly assigned.

For single images and video, the problem has been mainly tackled by regressing the parameters of the SMPL [57] body model [14, 20, 22, 25, 38, 83, 84, 87, 108, 109, 111, 112]. Although this can work robustly with as little as one view, the reconstructions are very coarse and cannot explain hair, clothing, and fine geometric details. The only

exception is the work of Mustafa *et al.* [61], which performs model-free reconstruction of multiple humans by combining an explicit voxel-based representation with an implicit function refinement. However, the method requires training on a large synthetic dataset of multiple people which hinders generalization. Our work, on the other hand, performs 3D reconstructions, produces renderings of novel views, and can generalize to arbitrary multi-human scenes.

Multi-view capture setups can help resolve depth ambiguities and some of the occlusions. Classic methods for estimating multiple humans rely heavily on segmentation masks and template mesh tracking [54, 55, 96]. We avoid the use of segmentation masks by adopting volumetric rendering for implicit surfaces [90]. More recently, deep learning-based approaches were proposed, but they either require temporal information [30, 80, 115, 116], pre-training on a large dataset [116] which cannot work on general scenes, or a coarse body model [30, 80, 115] which lacks geometric detail. Here, we focus on the multi-human setting on static scenes and propose a method that recovers accurate reconstructions and at the same time produces renderings of novel viewpoints.

Neural Surface Reconstruction and Novel-View Synthesis.

For generating free-viewpoint video, image-based rendering has been considered as an alternative or complement to 3D reconstruction [10, 46, 52, 52, 73, 93, 98, 99]. When geometry proxies are available, neural rendering [1, 35, 86] can produce competitive novel view synthesis. Recently, NeRF[59] demonstrated impressive rendering results by representing a 3D scene as a neural radiance field, trained only with calibrated multi-view images through the use of volume rendering. However, due to the unconstrained volumetric representation and self-supervised training on RGB values, reconstructed geometries tend to be too noisy to be useful for 3D applications. To recover more accurate 3D geometry along with appearance, DVR [63], IDR [101], and NLR [42] propose to learn an implicit representation directly from multi-view images but require accurate object masks to work. To avoid the need for segmentation masks, recent works propose to combine implicit representations with volume rendering [64, 90, 100]. These methods show remarkable reconstruction results but struggle when the number of input views is low. Implicit neural representations from sparse input can be obtained by using pre-trained pixel-aligned features or 3D feature volumes for input images [4, 27, 28, 34, 36, 48, 78, 79, 103] or point clouds [8, 13, 31, 51, 65, 67, 68, 74, 75, 94], but this requires ground-truth geometry and is limited by the training data, struggling to generalize to new scenes. Sparse variants that do not require generalizable features were proposed in the image input *e.g.* [43, 49, 56, 62, 102] and point cloud input case *e.g.* [11, 66, 69, 70, 95]. InfoNeRF [43] regu-

larizes sparse views by adding an entropy constraint on the density of the rays, RegNeRF [62] uses a patch-based regularizer over generated depth maps, and SparseNeuS [56] uses a multi-scale approach along with learned features that are fine-tuned on each scene. Our approach builds on NeuS [90], and tackles the sparse view challenge by adding human-specific geometric priors and novel regularizations.

3. Method

Given a sparse set of views $\{I_i\}_{i=1}^N$ of a multi-human scene with camera intrinsics and extrinsics $\{K_i, [R|t]_i\}$, our goal is to reconstruct geometry and synthesize the appearance of multiple humans from arbitrary viewpoints. The pipeline is illustrated in Fig. 12. Our approach builds on NeuS [90], which combines an implicit signed distance representation for geometry with volumetric rendering. In order to solve the challenging case of multiple humans occluding each other, we hypothesize that a naive RGB reconstruction loss is insufficient and propose to use a strong geometric prior before training with multi-view images. Towards this, we first train the implicit SDF network independently by leveraging off-the-shelf SMPL estimations (Sec. 3.2). To handle details and represent appearance, the geometry network is then fine-tuned considering foreground and background objects. Moreover, we propose the use of hybrid bounding box rendering to handle the multi-human setting (Sec. 3.3). Additionally, we define an explicit SDF constraint based on the uncertainty of the SMPL estimations, together with a ray consistency loss, and a saturation loss to improve image rendering quality for sparse views (Sec. 3.4).

3.1. Scene Representation and Rendering

We define a multi-human surface \mathcal{S} as the zero-level set of a signed distance function (SDF) $f_{\theta_0} : \mathbb{R}^3 \rightarrow \mathbb{R}$, encoded by a Multilayer Perceptron (MLP) f_{θ_0} with parameters θ_0 :

$$\mathcal{S} = \{p \in \mathbb{R}^3 | f_{\theta_0}(p) = 0\}. \quad (1)$$

Following NeuS [90], we train the geometry network f_{θ_0} along with a color network c_{θ_1} , with parameters θ_1 , mapping a point p to color values (more details in Sec. 3.3). Combining the SDF representation with volume rendering, we approximate the color along a ray r by:

$$C(r) = \sum_{i=1}^N w(p_i) c_{\theta_1}(p_i), \quad (2)$$

$$w(p_i) = T(p_i) \alpha(p_i), \quad (3)$$

$$T(p_i) = \prod_j^{i-1} (1 - \alpha(p_j)), \quad (4)$$

where $p_i = o + t_i v$ is a sampled point along the ray r starting at camera center o with direction v ; $c_{\theta_1}(p_i)$ is the predicted color at p_i , $w(p_i)$ is the weight function, $T(p_i)$ is the

accumulated transmittance, and $\alpha(p_i)$ is the opacity value. Following NeuS, $\alpha(p_i)$ is defined as a function of the signed distance representation:

$$\alpha(p_i) = \max \left(\frac{\Phi(f_{\theta_0}(p_i)) - \Phi(f_{\theta_0}(p_{i+1}))}{\Phi(f_{\theta_0}(p_i))}, 0 \right) \quad (5)$$

where $f_{\theta_0}(p_i)$ is the signed distance of p_i , $\Phi(f_{\theta_0}(x)) = (1 + e^{-sx})^{-1}$ is the cumulative distribution function (CDF) of the logistic distribution, and s is a learnable parameter (see [90] for more details).

3.2. Geometric Prior

Typically, the SDF function f_{θ_0} and the color function c_{θ_1} are simultaneously optimized by minimizing the difference between the rendered and ground-truth RGB values [59, 90, 101]. While this allows to train without the need for geometric supervision, it has been noted that a photometric error alone is insufficient for the challenging sparse-view setting [18, 77], since there are not enough images to compensate for the inherent ambiguity in establishing correspondences between views. For the *multi-human* setting this becomes more problematic, as correspondences are even more ambiguous due to clutter.

To address this, we propose to regularize using geometric information by first independently training f_{θ_0} using off-the-shelf SMPL fittings, which can be robustly computed from the input data. We train this network in a supervised manner by sampling points with their distance values as in [71]. Given that SMPL can only coarsely represent the real surface, we treat this geometry as a “noisy” estimate that will be later improved upon using the multi-view images. Preparing for this, and inspired by [18, 77], we model the SMPL “noise” as a Gaussian distribution $\mathcal{N}(0, s_{noise}(p_j)^2)$ with standard deviation $s_{noise}(p_j)$, and train f_{θ_0} to output an estimate of the uncertainty $s_{noise}(p_j)$ along with the distance value; that is, $f_{\theta_0}(p_j) = (d_j, s_{noise})$. The geometry network f_{θ_0} is then optimized by minimizing the negative log-likelihood of a Gaussian:

$$\mathcal{L}_s = \frac{1}{n} \sum_{j=1}^n \left(\log(s_{noise}(p_j)^2) + \frac{(d_j - d'_j)^2}{s_{noise}(p_j)^2} \right), \quad (6)$$

where n is the number of sampled points, d_j is the predicted SDF value for point p_j , and d'_j is the signed distance sampled directly from the SMPL meshes.

3.3. Hybrid Rendering with Geometry Constraints

To work with unbounded scenes, NeRF++ [113] proposed to separately model the foreground and background geometries using an inverted sphere parameterization, where the foreground is parameterized within an inner unit sphere, and the rest is represented by an inverted sphere covering the

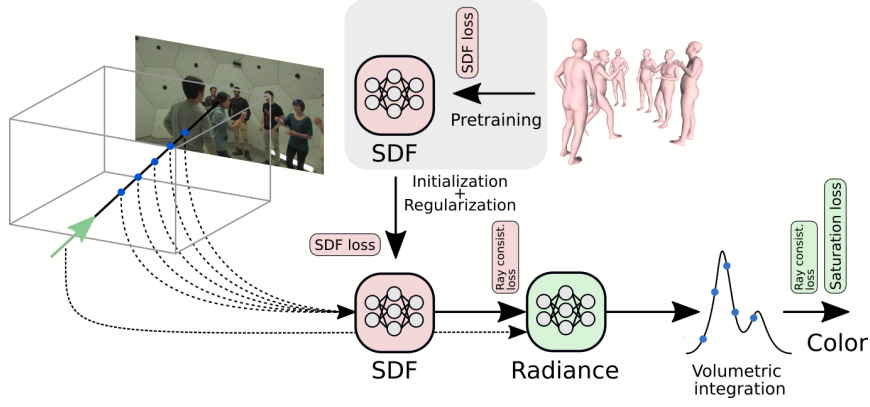


Figure 1. **Overview.** We address the multi-human implicit shape and appearance learning problem by initializing the geometry using SMPL (Sec. 3.2), along with uncertainty-based SDF supervision and novel photometric regularizations designed to compensate for the lack of views (Sec. 3.4). We also model the foreground (Union of SMPL bounding boxes) and remainder of the scene separately (Sec. 3.3).

complement of the inner volume. We follow this and train separate models for foreground and background. Specifically, we use a simple NeRF [59] architecture for the background and train the foreground model using f_{θ_0} and the color network c_{θ_1} , where the output color $C(p_i)$ is predicted as:

$$C(p_i) = c_{\theta_1}(\gamma(p_i), \gamma(v_i), f_0, f_1). \quad (7)$$

Here, $\gamma(p_i)$ and $\gamma(v_i)$ are the positional encodings [59, 85] of the sampled point p_i and its ray direction v_i , and f_0 includes the gradients of predicted SDF and predicted feature from the geometry network f_{θ_0} [101]. Additionally, to inject geometric prior knowledge into the appearance network we condition c_{θ_1} on the rasterized depth feature from the corresponding SMPL mesh.

For reconstructing multiple humans, one difficulty in modeling the foreground as in NeRF++ is that the bounding sphere will contain a large empty space, making it costly to search for the surface during hierarchical sampling and adding non-relevant points to the training. To resolve this, we propose to use instead multiple 3D bounding boxes as the foreground volume. Specifically, we define a bounding box B^j for the j -th human using the SMPL fittings, with minimum and maximum coordinates $[B_{min}^j - \delta, B_{max}^j + \delta]$, where B_{min}^j and B_{max}^j are the minimum and maximum coordinates of SMPL along the x, y, z axes respectively, and δ is a spatial margin (here we set to 0.1). The foreground volume is then defined as $B = \cup_{j=1..M} B^j$, and we define $b(p_i)$ as

$$b(p_i) = \begin{cases} 1, & p_i \in B, \\ 0, & p_i \notin B \end{cases} \quad (8)$$

For points that fall inside the foreground, $p \in B$, we calculate the opacity value $\alpha^{FG}(p_i)$ using the predictions of $f_{\theta_0}(p_i)$ according to Eq. 5, and the color $C(p_i)^{FG}$ using c_{θ_1} . The points that fall outside the bounding box are modeled as background using a NeRF model, where the opacity is calculated as $\alpha^{BG}(p_i) = 1 - e^{\sigma(p_i)\delta(p_i)}$, with δ and σ defined as in [59], and the color C^{BG} is predicted using α^{BG} .

Given a point p_i , its color and opacity values are updated as follows:

$$C(p_i) = b(p_i)C^{FG}(p_i) + (1 - b(p_i))C^{BG}(p_i) \quad (9)$$

$$\alpha(p_i) = b(p_i)\alpha^{FG}(p_i) + (1 - b(p_i))\alpha^{BG}(p_i) \quad (10)$$

Finally, following [5], given a ray r with n sampled points $\{p_i = o + t_i v\}_{i=1}^n$, the color is approximated as:

$$C(r) = \frac{\sum_{i=1}^N W(p_i)C(p_i)}{\sum_{i=1}^N W(p_i)}, \quad (11)$$

where $W(p_i) = T(p_i)\alpha(p_i)$, $T(p_i) = \prod_{j=1}^{i-1} (1 - \alpha(p_j))$. This function allocates higher weights to points near the surface and lower weights to points away from the surface, and is used to improve the rendering quality.

3.4. Optimization

Given a set of multi-view images, and a pre-trained SDF network f'_{θ_0} (Sec. 3.2), we minimize the following objective:

$$\mathcal{L} = \mathcal{L}_r + \lambda_{eik}\mathcal{L}_{eik} + \lambda_{sdf}\mathcal{L}_{sdf} + \lambda_r\mathcal{L}_r + \lambda_s\mathcal{L}_s, \quad (12)$$

where \mathcal{L}_r is a L1 reconstruction loss between the rendered image I_r and the ground-truth I'_r and \mathcal{L}_{eik} is the Eikonal loss [24].

Additionally, we propose to use an uncertainty-based SDF loss \mathcal{L}_{sdf} , a novel ray consistency loss \mathcal{L}_r and saturation loss \mathcal{L}_s which are explained in the following.

SDF Loss. As detailed in Sec. 3.2, we treat the SMPL mesh as a noisy estimate of the real surface. When the sampled points are not within the foreground box B , or the absolute sdf value predicted by the geometry network f_{θ_0} is greater than a pre-defined threshold ξ_0 , or the standard deviation $s_j = s_{noise}(p)_j$ is bigger than the threshold ξ_1 , we

use the following loss:

$$\mathcal{L}_{\text{sdf}} = \begin{cases} \frac{1}{n} \sum_{j=1}^n (\log(s_j^2) + \frac{(d'_j - d_j)^2}{s_j^2}), \\ s.t. (p_i \notin B, |d_j| > \xi_0 \text{ or } s_j > \xi_1) \\ 0, \text{ otherwise} \end{cases} \quad (13)$$

where d_j and d'_j are the SDF predictions from the final f_{θ_0} and initial network \tilde{f}_{θ_0} , and ξ_0, ξ_1 are set to 0.2 and 0.5, respectively. This function encourages the network to maintain geometry consistency during learning while allowing some freedom to learn the details encoded in the images.

Ray Consistency Loss. We introduce the following ray consistency loss \mathcal{L}_r to ensure photometric consistency across all images under sparse views:

$$\mathcal{L}_r = \|C(r_i) - C(r^*)\|_1 + D_{KL}(P(r_i) \| P(r^*)) \quad (14)$$

where $C(r_i)$ is the ground truth color of a randomly sampled ray r_i on a small patch and $C(r^*)$ denotes the rendered color of an interpolated ray on a small patch. Inspired by [43], we introduce a KL-divergence regularization for the ray density, where $P(r_i) = \frac{\alpha_i}{\sum_{i=1}^N \alpha_i}$. The goal of this loss is to ensure consistency and smoothness of unseen rays by constraining the interpolated rays on a small patch to have a similar distribution, both for color and density.

Saturation Loss. Finally, we observe that real-world images might contain variable illumination or transient occluders among different views (this is the case for example in the CMU Panoptic dataset [40, 81]), which can degrade the rendering quality due to inconsistency across views. Instead of learning complex transient embeddings as in [58], we propose to simply convert the RGB image into the HSV space, and calculate the L1 reconstruction loss of the saturation value between the rendered image and the ground truth: $\mathcal{L}_s = \|I_s - I_s^{gt}\|_1$.

4. Results

In this section we provide implementation details (Sec. 4.1), and demonstrate our performance against baselines on real (Sec. 4.2) and synthetic (Sec. 4.3) datasets, in terms of novel-view synthesis, visual reconstructions, and geometry error. Finally, we show ablation studies (Sec. 4.4) that demonstrate the importance of each of the proposed components.

4.1. Implementation Details

Our method was implemented using PyTorch [72], and trained on a Quadro RTX 5000 GPU. We use ADAM optimizer [44] with a learning rate ranging from 5×10^{-4} to

2.5×10^{-5} , controlled by cosine decay schedule. Our network architecture follows [59, 101]. For a fair comparison, we sample 256 rays per batch and follow the coarse and fine sampling strategy of [90]. More network structure and training details are shown in the supplementary material.

4.2. Real Multi-Human Dataset

We first evaluate our approach on the CMU Panoptic Dataset [40, 81]. Our experiments were performed on five different scenes, where each scene originally includes 30 views containing 3/4/5/6/7 people. The training views were randomly extracted from the HD sequences ‘Ultimatum’ and ‘Haggling’. We uniformly choose 5/10/15/20 views for training and the rest 25/20/15/10 views for testing. We compare with two major baselines: NeuS [90] and VolSDF[100], both in terms of novel-view synthesis and geometry reconstructions (qualitatively). For quantitative evaluation, we report three commonly used image metrics: peak signal-to-noise ratio (PSNR) [29], structural similarity index (SSIM) [92] and learned perceptual image patch similarity (LPIPS) [114]. For qualitative comparison, both rendered images and rendered normal images are shown.

Comparison with baselines. Tab. 1 demonstrates novel view synthesis results with different training views (5/10/15/20) compared to the baselines. Our proposed method outperforms these in PSNR and SSIM in all the scenes, and consistently performs better or equal in terms of LPIPS. For qualitative comparison, we demonstrate both rendered novel views and normal images in Fig. 8. As seen here, when given 5/10 training views the baseline methods fail to reconstruct a good geometry or render a realistic appearance. Although the quality of the geometries improves with 15/20 training views, the results exhibit missing body parts or can mix the background with the subjects. On the other hand, our method can reconstruct a complete geometry for all humans in all sparse-view cases.

Fig. 3 additionally shows the relationship between the number of training views and the quality of the synthesized images. The fewer the number of views, the harder it is for all methods to reconstruct high-quality images, whereas our approach is more robust to fewer training views. For denser inputs (e.g. more than 20 views), our method reaches similar albeit slightly better performance than the baselines, since the proposed work focuses on sparse scenarios.

Comparison to single human NeRF. We compare our method to the single human nerf state-of-the-art method ARAH [91]. We note that adapting such methods to our setup requires tedious manual pre-processing (detecting and segmenting people, associating detections across views), which is not required by our approach. We run a separate ARAH model for each person in the scene using 5 training images (see supp. mat.). Fig. 4 shows novel view and reconstruction results. Learning for each person separately

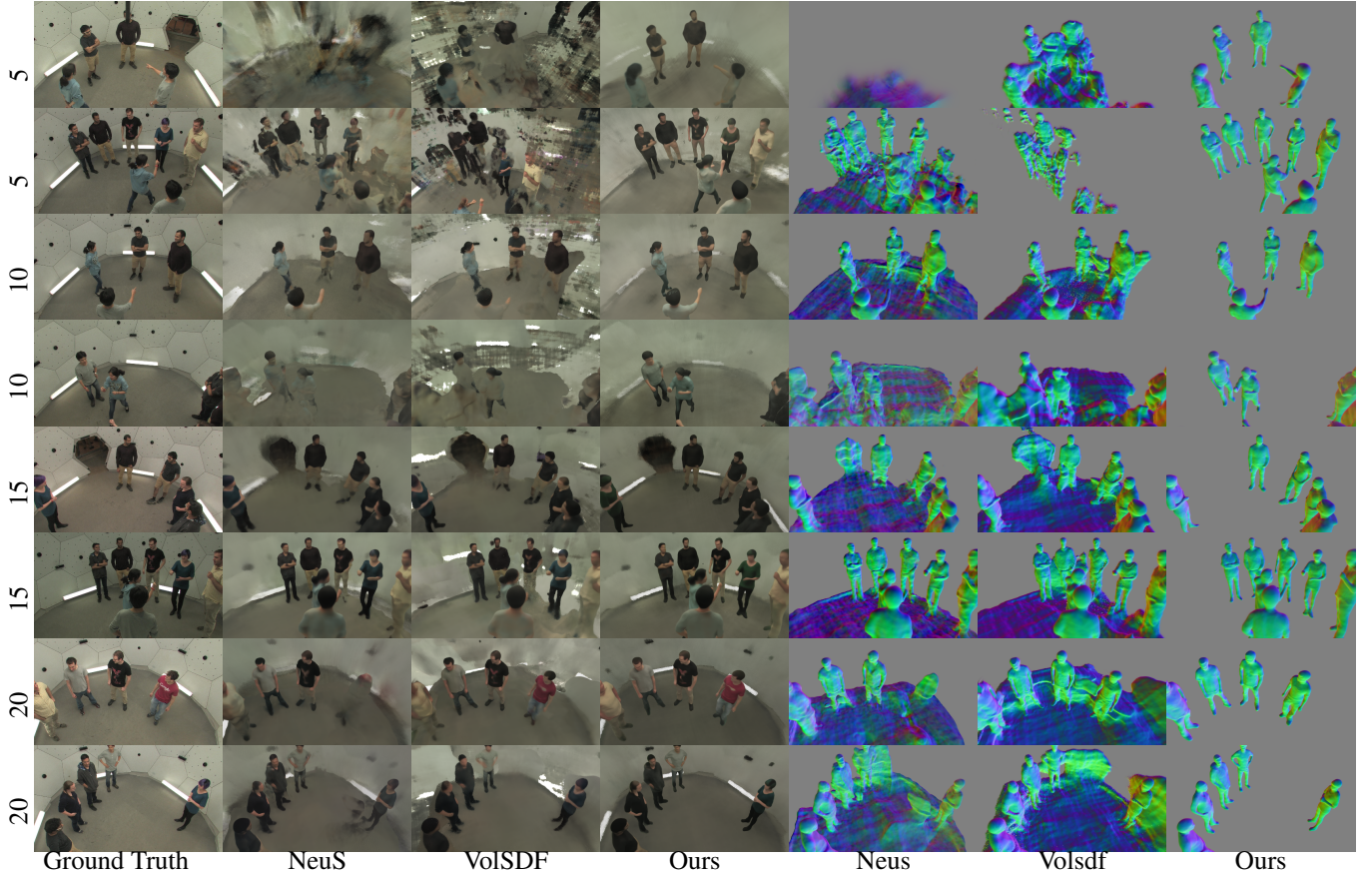


Figure 2. Qualitative comparison against NeuS [90] and VolSDF [100] of synthesised novel views and reconstructed normal images of multiple humans on CMU Panoptic dataset [40, 81], using 5/10/15/20 training views.

Scene	Method	PSNR \uparrow				SSIM \uparrow				LPIPS \downarrow			
		5	10	15	20	5	10	15	20	5	10	15	20
1	NeuS	17.83	18.84	19.39	21.97	0.62	0.67	0.69	0.55	0.74	0.51	0.49	0.45
	VolSDF	17.50	18.08	19.51	22.31	0.64	0.61	0.67	0.71	0.61	0.54	0.51	0.48
	Ours	18.41	20.32	21.60	23.19	0.67	0.73	0.73	0.74	0.55	0.50	0.50	0.49
2	NeuS	16.87	18.51	19.40	21.05	0.60	0.65	0.70	0.71	0.57	0.53	0.51	0.49
	VolSDF	16.36	17.52	19.40	21.60	0.57	0.59	0.67	0.70	0.62	0.53	0.49	0.47
	Ours	19.72	21.15	21.40	23.12	0.70	0.73	0.73	0.74	0.50	0.49	0.48	0.47
3	NeuS	16.03	17.39	19.17	21.21	0.56	0.61	0.70	0.73	0.62	0.54	0.47	0.46
	VolSDF	16.36	18.21	19.56	21.06	0.57	0.59	0.64	0.68	0.62	0.52	0.48	0.47
	Ours	18.57	20.94	21.86	23.16	0.66	0.73	0.74	0.74	0.52	0.48	0.47	0.47
4	NeuS	14.16	17.14	19.87	21.37	0.49	0.51	0.70	0.72	0.60	0.57	0.48	0.46
	VolSDF	13.51	17.07	18.68	20.89	0.50	0.57	0.65	0.68	0.64	0.54	0.53	0.46
	Ours	19.54	20.94	21.35	23.29	0.69	0.72	0.73	0.75	0.50	0.47	0.47	0.45
5	NeuS	17.69	18.60	20.03	21.50	0.57	0.62	0.69	0.70	0.55	0.54	0.50	0.47
	VolSDF	14.85	17.32	19.04	20.91	0.53	0.57	0.66	0.68	0.63	0.58	0.53	0.48
	Ours	19.34	20.55	21.08	22.55	0.67	0.70	0.72	0.72	0.51	0.47	0.47	0.47
Average	NeuS	16.52	17.79	19.57	21.42	0.57	0.62	0.69	0.72	0.58	0.54	0.49	0.47
	VolSDF	15.81	17.68	19.23	21.35	0.56	0.59	0.66	0.69	0.62	0.54	0.50	0.47
	Ours	19.12	20.78	21.46	23.06	0.68	0.72	0.73	0.74	0.52	0.48	0.48	0.47

Table 1. Comparison against NeuS [90] and VolSDF [100] on the CMU Panoptic dataset [40, 81], using 5/10/15/20 views for training.

implies providing erroneous supervision to the model whenever the person is occluded in the scene or segmentation masks are not accurate. As a result, ARAH’s renderings and geometry display many artifacts compared to our results.

Conversely, our method avoids this by learning through rendering the union of SMLP bounding boxes conjointly. We also noticed that ARAH’s results are very sensitive to the sparsity and choice of the training views.

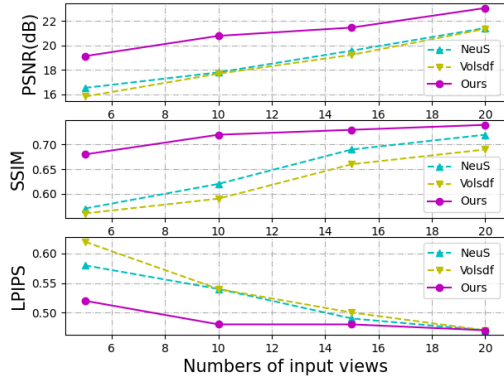


Figure 3. Quantitative comparison of average PSNR (↑), SSIM (↑) and LPIPS (↓) with increased number of training views.

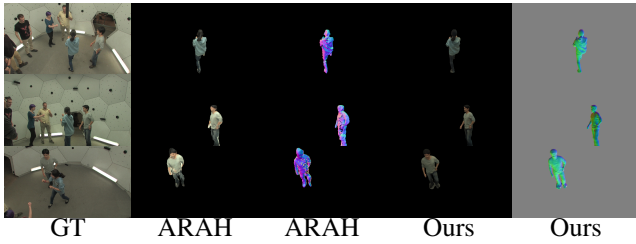


Figure 4. Comparison against [91] from 5 training views. PSNRs for the 3 examples are respectively: 26.97/29.56, 27.48/33.66, 24.36/30.56 (ARAH/Ours).

Scene	Method	PSNR↑	SSIM↑	LPIPS↓
1	InfoNeRF	14.64	0.50	0.64
	NeuS w/ info	17.98	0.65	0.58
	Ours	18.41	0.67	0.55
2	InfoNeRF	14.21	0.49	0.63
	NeuS w/ info	18.21	0.64	0.57
	Ours	19.72	0.70	0.50
3	InfoNeRF	13.78	0.45	0.63
	NeuS w/ info	16.31	0.59	0.60
	Ours	18.57	0.66	0.52
4	InfoNeRF	12.26	0.41	0.68
	NeuS w/ info	14.42	0.51	0.60
	Ours	19.54	0.69	0.50
5	InfoNeRF	12.17	0.45	0.63
	NeuS w/ info	17.89	0.60	0.61
	Ours	19.34	0.67	0.51
Ave	InfoNeRF	13.61	0.46	0.64
	NeuS w/ info	16.96	0.60	0.59
	Ours	19.12	0.68	0.52

Table 2. Comparison against sparse-view NeRF approaches: InfoNeRF [43] and NeuS with InfoNeRF’s regularizations, on the CMU Panoptic dataset [40, 81] using 5 training views.

Comparison with sparse NeRF. We further compare with a recent NeRF method that was specifically designed to handle sparse views, namely InfoNeRF [43]. We compare both against the original InfoNeRF, and a version of NeuS

trained with InfoNeRF’s regularization. For this experiment, we use again the CMU Panoptic dataset [40, 81] with five training views. Tab. 6 shows that, compared to InfoNeRF and NeuS with InfoNeRF’s regularization, our method improves the rendering quality in all of the scenes.

4.3. Synthetic Dataset

Based on the MultiHuman-Dataset [105, 116], we used Unity 3D to create a synthetic dataset with 29 cameras arranged in a great circle. This includes three scenes with similar backgrounds but different camera locations and orientations. Each of the scenes contains 1/5/10 humans respectively. We train with 5/10/15 views on each scene and test with 14 fixed views. Tab. 3 reports the average error for all testing views in PSNR, SSIM and LPIPS metrics. Our method reaches state-of-the-art performance on synthesized novel-view results. Fig. 5 shows generated novel views and corresponding normal images using 10/15 training images. Our approach can reconstruct complete geometry of all humans in the scene, while the baseline methods might miss some of the people when they have similar color with the background, *e.g.* the shadow area in Fig. 5.

In the 5/10 input views case, the baseline methods usually fail to reconstruct the full geometry of humans due to the sparse inputs. Thus, we report Chamfer distance in Tab. 3 only for the 15-views case. Since the baseline methods usually contain extra floor, for a fair comparison, we sample points from ground-truth meshes and compute the distance towards the reconstructed mesh for all methods. We report the bi-directional Chamfer distance in the supplementary material. Tab. 3 shows that, with an increasing number of humans in the scene, the quality of the reconstructed geometry of all methods decreases. However, compared with the baselines, our method can better handle multiple human scenes, achieving an order of magnitude less error.

4.4. Ablation Study

To prove the effectiveness of our proposed components we performed ablation studies on the CMU Panoptic dataset [40, 81]. We demonstrate quantitative comparisons in Tab. 4 and qualitative results in Fig. 6. We test the following settings:

Without geometry regularization (“w/o geometry”). We compare our full model against the model without geometry regularization (Sec. 3.2) and SDF uncertainty regularization (Eq. 13). We can see here that, although the method is still capable of isolating humans thanks to the bounding box rendering, both geometry and novel views are much less accurate, and the rendered images exhibit background artifacts and overly smooth results.

Without ray consistency loss (“w/o ray loss”). Here we remove the proposed ray consistency loss, without which



Figure 5. Qualitative comparison of synthesised novel views and reconstructed normal images on the synthetic dataset (MultiHuman-Dataset [116]) with 10 and 15 training views respectively.

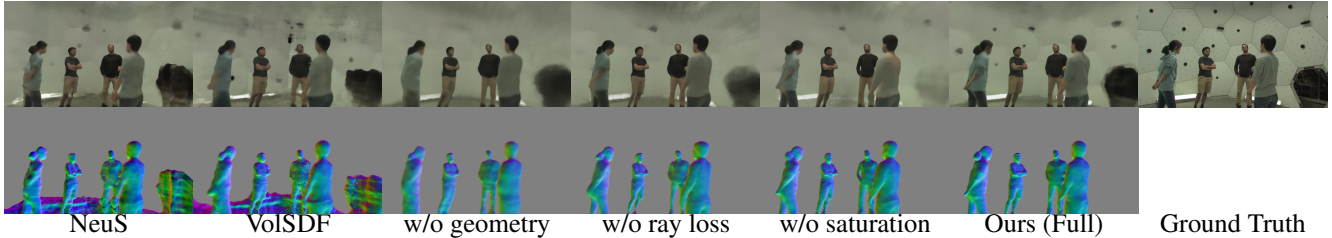


Figure 6. Ablation study on CMU Panoptic dataset [40, 81]. Comparison against our method without geometric regularization (w/o geometry), our method without ray consistency regularization (w/o ray loss), and our method without saturation regularization (w/o saturation).

# Humans	Method	PSNR \uparrow			SSIM \uparrow			LPIPS \downarrow			Chamfer \downarrow
		5	10	15	5	10	15	5	10	15	
1	NeuS	14.04	17.89	23.25	0.63	0.72	0.84	0.55	0.53	0.44	0.308
	VolSDF	13.93	21.75	25.89	0.61	0.81	0.86	0.55	0.51	0.44	0.019
	Ours	15.36	23.85	26.28	0.65	0.84	0.87	0.55	0.43	0.41	0.018
5	NeuS	14.15	18.14	18.54	0.61	0.72	0.72	0.54	0.46	0.44	0.321
	VolSDF	12.97	15.11	18.59	0.58	0.63	0.73	0.56	0.55	0.47	0.151
	Ours	17.63	20.10	20.33	0.71	0.79	0.77	0.47	0.40	0.40	0.020
10	NeuS	14.09	15.69	19.27	0.58	0.65	0.75	0.52	0.48	0.42	0.383
	VolSDF	12.66	16.99	19.30	0.56	0.70	0.77	0.56	0.50	0.41	0.248
	Ours	16.52	18.39	21.01	0.65	0.71	0.80	0.50	0.44	0.37	0.043
Average	NeuS	14.09	17.24	20.35	0.60	0.70	0.77	0.54	0.49	0.43	0.337
	VolSDF	13.18	17.95	21.26	0.58	0.71	0.79	0.56	0.52	0.44	0.139
	Ours	16.50	20.78	22.54	0.67	0.78	0.81	0.51	0.42	0.39	0.026

Table 3. Comparison against NeuS [90] and VolSDF [100] on the synthetic dataset, for different number of humans in the scene. We measure novel-view synthesis quality in terms of PSNR, SSIM and LPIPS, as well as geometry error in terms of Chamfer distance.

the average rendering quality also degrades.

Without saturation loss. Finally, we remove the saturation loss from our methods, which decreases by about 0.5 in PSNR on average. Fig. 6 shows that, without this, the image tone can contain artifacts due to changes in lighting (see for example the back of the rightmost subject).

5. Conclusion

We presented an approach for novel view synthesis of multiple humans from a sparse set of input views. To achieve this, we proposed geometric regularizations that improve geometry training by leveraging a pre-computed SMPL model, along with a patch-based ray consistency loss and a saturation loss that help with novel-view renderings in the sparse-

Method	PSNR \uparrow		SSIM \uparrow		LPIPS \downarrow	
	5	15	5	15	5	15
Neus [90]	16.87	19.40	0.60	0.70	0.51	0.53
Volsdf[100]	16.03	19.40	0.53	0.67	0.60	0.49
w/o Geometry	17.54	20.28	0.60	0.70	0.53	0.48
w/o Ray loss	19.07	20.95	0.67	0.72	0.52	0.47
w/o Saturation	18.95	20.92	0.65	0.72	0.54	0.49
Ours(Full)	19.72	21.40	0.70	0.73	0.50	0.48

Table 4. Ablation study on the CMU Panoptic dataset [40, 81] with 5/15 training views respectively. Comparison against our method without geometric regularization (w/o Geometry), without ray consistency regularization (w/o Ray loss), and without saturation regularization (w/o Saturation).

view setting. Our experiments showed state-of-the-art performance for multiple human geometry and appearance reconstruction on real multi-human dataset (CMU Panoptic [40, 81]) and on synthetic data (MultiHuman-Dataset [116]). Our method still has several limitations. For instance, our method does not model close human interactions, as this is a much more challenging case. Addressing this is an interesting direction for future work.

References

- [1] Kara-Ali Aliev, Artem Sevastopolsky, Maria Kolos, Dmitry Ulyanov, and Victor Lempitsky. Neural point-based graphics. In *European Conference on Computer Vision*, pages 696–712. Springer, 2020. 2
- [2] Thiemo Alldieck, Marcus Magnor, Weipeng Xu, Christian Theobalt, and Gerard Pons-Moll. Detailed human avatars from monocular video. In *2018 International Conference on 3D Vision (3DV)*, pages 98–109. IEEE, 2018. 1
- [3] Thiemo Alldieck, Marcus Magnor, Weipeng Xu, Christian Theobalt, and Gerard Pons-Moll. Video based reconstruction of 3d people models. In *Proceedings of the IEEE Conference on Computer Vision and Pattern Recognition*, pages 8387–8397, 2018. 2
- [4] Thiemo Alldieck, Mihai Zanfir, and Cristian Sminchisescu. Photorealistic monocular 3d reconstruction of humans wearing clothing. In *Proceedings of the IEEE/CVF Conference on Computer Vision and Pattern Recognition*, pages 1506–1515, 2022. 2
- [5] Dejan Azinović, Ricardo Martin-Brualla, Dan B Goldman, Matthias Nießner, and Justus Thies. Neural rgb-d surface reconstruction. In *Proceedings of the IEEE/CVF Conference on Computer Vision and Pattern Recognition*, pages 6290–6301, 2022. 4
- [6] Alexandru O Balan, Leonid Sigal, Michael J Black, James E Davis, and Horst W Haussecker. Detailed human shape and pose from images. In *2007 IEEE Conference on Computer Vision and Pattern Recognition*, pages 1–8. IEEE, 2007. 2
- [7] Federica Bogo, Angjoo Kanazawa, Christoph Lassner, Peter Gehler, Javier Romero, and Michael J Black. Keep it simple: Automatic estimation of 3d human pose and shape from a single image. In *European conference on computer vision*, pages 561–578. Springer, 2016. 2
- [8] Alexandre Boulch and Renaud Marlet. Poco: Point convolution for surface reconstruction. In *Proceedings of the IEEE/CVF Conference on Computer Vision and Pattern Recognition*, pages 6302–6314, 2022. 2
- [9] Andrei Burov, Matthias Nießner, and Justus Thies. Dynamic surface function networks for clothed human bodies. In *Proceedings of the IEEE/CVF International Conference on Computer Vision*, pages 10754–10764, 2021. 2
- [10] Joel Carranza, Christian Theobalt, Marcus A Magnor, and Hans-Peter Seidel. Free-viewpoint video of human actors. *ACM transactions on graphics (TOG)*, 22(3):569–577, 2003. 2
- [11] Chao Chen, Zhizhong Han, and Yu-Shen Liu. Unsupervised inference of signed distance functions from single sparse point clouds without learning priors. In *Proceedings of the IEEE/CVF Conference on Computer Vision and Pattern Recognition (CVPR)*, 2023. 2
- [12] Jianchuan Chen, Ying Zhang, Di Kang, Xuefei Zhe, Linchao Bao, Xu Jia, and Huchuan Lu. Animatable neural radiance fields from monocular rgb videos. *arXiv preprint arXiv:2106.13629*, 2021. 1
- [13] Julian Chibane, Thiemo Alldieck, and Gerard Pons-Moll. Implicit functions in feature space for 3d shape reconstruction and completion. In *Proceedings of the IEEE/CVF Conference on Computer Vision and Pattern Recognition*, pages 6970–6981, 2020. 2
- [14] Hongsuk Choi, Gyeongsik Moon, Joonkyu Park, and Kyoung Mu Lee. Learning to estimate robust 3d human mesh from in-the-wild crowded scenes. In *Proceedings of the IEEE/CVF Conference on Computer Vision and Pattern Recognition*, pages 1475–1484, 2022. 1, 2
- [15] Vasileios Choutas, Georgios Pavlakos, Timo Bolkart, Dimitrios Tzionas, and Michael J Black. Monocular expressive body regression through body-driven attention. In *European Conference on Computer Vision*, pages 20–40. Springer, 2020. 1, 2
- [16] Alvaro Collet, Ming Chuang, Pat Sweeney, Don Gillett, Dennis Evseev, David Calabrese, Hugues Hoppe, Adam Kirk, and Steve Sullivan. High-quality streamable free-viewpoint video. *ACM Transactions on Graphics (ToG)*, 34(4):1–13, 2015. 1, 2
- [17] Edilson De Aguiar, Carsten Stoll, Christian Theobalt, Naveed Ahmed, Hans-Peter Seidel, and Sebastian Thrun. Performance capture from sparse multi-view video. In *ACM SIGGRAPH 2008 papers*, pages 1–10. 2008. 2
- [18] Kangle Deng, Andrew Liu, Jun-Yan Zhu, and Deva Ramanan. Depth-supervised nerf: Fewer views and faster training for free. In *Proceedings of the IEEE/CVF Conference on Computer Vision and Pattern Recognition*, pages 12882–12891, 2022. 2, 3
- [19] Zijian Dong, Chen Guo, Jie Song, Xu Chen, Andreas Geiger, and Otmar Hilliges. Pina: Learning a personalized implicit neural avatar from a single rgb-d video sequence. In *Proceedings of the IEEE/CVF Conference on Computer Vision and Pattern Recognition*, pages 20470–20480, 2022. 1
- [20] Zijian Dong, Jie Song, Xu Chen, Chen Guo, and Otmar Hilliges. Shape-aware multi-person pose estimation from multi-view images. In *Proceedings of the IEEE/CVF International Conference on Computer Vision*, pages 11158–11168, 2021. 2
- [21] Mingsong Dou, Sameh Khamis, Yury Degtyarev, Philip Davidson, Sean Ryan Fanello, Adarsh Kowdle, Sergio Orts Escolano, Christoph Rhemann, David Kim, Jonathan Taylor, et al. Fusion4d: Real-time performance capture of challenging scenes. *ACM Transactions on Graphics (ToG)*, 35(4):1–13, 2016. 2
- [22] Mihai Fieraru, Mihai Zanfir, Elisabeta Oneata, Alin-Ionut Popa, Vlad Olaru, and Cristian Sminchisescu. Three-dimensional reconstruction of human interactions. In *Proceedings of the IEEE/CVF Conference on Computer Vision and Pattern Recognition*, pages 7214–7223, 2020. 1, 2
- [23] Juergen Gall, Carsten Stoll, Edilson De Aguiar, Christian Theobalt, Bodo Rosenhahn, and Hans-Peter Seidel. Motion

- capture using joint skeleton tracking and surface estimation. In *2009 IEEE Conference on Computer Vision and Pattern Recognition*, pages 1746–1753. Ieee, 2009. 2
- [24] Amos Gropp, Lior Yariv, Niv Haim, Matan Atzmon, and Yaron Lipman. Implicit geometric regularization for learning shapes. *arXiv preprint arXiv:2002.10099*, 2020. 4
- [25] Riza Alp Guler and Iasonas Kokkinos. Holopose: Holistic 3d human reconstruction in-the-wild. In *Proceedings of the IEEE/CVF Conference on Computer Vision and Pattern Recognition*, pages 10884–10894, 2019. 2
- [26] Kaiwen Guo, Peter Lincoln, Philip Davidson, Jay Busch, Xueming Yu, Matt Whalen, Geoff Harvey, Sergio Orts-Escolano, Rohit Pandey, Jason Dourgarian, et al. The relightables: Volumetric performance capture of humans with realistic relighting. *ACM Transactions on Graphics (ToG)*, 38(6):1–19, 2019. 1, 2
- [27] Tong He, John Collomosse, Hailin Jin, and Stefano Soatto. Geo-pifu: Geometry and pixel aligned implicit functions for single-view human reconstruction. *Advances in Neural Information Processing Systems*, 33:9276–9287, 2020. 2
- [28] Tong He, Yuanlu Xu, Shunsuke Saito, Stefano Soatto, and Tony Tung. Arch++: Animation-ready clothed human reconstruction revisited. In *Proceedings of the IEEE/CVF International Conference on Computer Vision*, pages 11046–11056, 2021. 2
- [29] Alain Hore and Djemel Ziou. Image quality metrics: Psnr vs. ssim. In *2010 20th international conference on pattern recognition*, pages 2366–2369. IEEE, 2010. 5
- [30] Buzhen Huang, Yuan Shu, Tianshu Zhang, and Yangang Wang. Dynamic multi-person mesh recovery from uncalibrated multi-view cameras. In *2021 International Conference on 3D Vision (3DV)*, pages 710–720. IEEE, 2021. 1, 2
- [31] Jiahui Huang, Zan Gojcic, Matan Atzmon, Or Litany, Sanja Fidler, and Francis Williams. Neural kernel surface reconstruction. In *Proceedings of the IEEE/CVF Conference on Computer Vision and Pattern Recognition*, pages 4369–4379, 2023. 2
- [32] Yinghao Huang, Federica Bogo, Christoph Lassner, Angjoo Kanazawa, Peter V Gehler, Javier Romero, Ijaz Akhter, and Michael J Black. Towards accurate marker-less human shape and pose estimation over time. In *2017 international conference on 3D vision (3DV)*, pages 421–430. IEEE, 2017. 2
- [33] Zeng Huang, Tianye Li, Weikai Chen, Yajie Zhao, Jun Xing, Chloe LeGendre, Linjie Luo, Chongyang Ma, and Hao Li. Deep volumetric video from very sparse multi-view performance capture. In *Proceedings of the European Conference on Computer Vision (ECCV)*, pages 336–354, 2018. 2
- [34] Zeng Huang, Yuanlu Xu, Christoph Lassner, Hao Li, and Tony Tung. Arch: Animatable reconstruction of clothed humans. In *Proceedings of the IEEE/CVF Conference on Computer Vision and Pattern Recognition*, pages 3093–3102, 2020. 2
- [35] Shubhendu Jena, Franck Multon, and Adnane Boukhayma. Neural mesh-based graphics. In *European Conference on Computer Vision*, pages 739–757. Springer, 2022. 2
- [36] Shubhendu Jena, Franck Multon, and Adnane Boukhayma. Geotransfer: Generalizable few-shot multi-view reconstruction via transfer learning. *arXiv preprint arXiv:2408.14724*, 2024. 2
- [37] Boyi Jiang, Yang Hong, Hujun Bao, and Juyong Zhang. Selfrecon: Self reconstruction your digital avatar from monocular video. In *Proceedings of the IEEE/CVF Conference on Computer Vision and Pattern Recognition*, pages 5605–5615, 2022. 1
- [38] Wen Jiang, Nikos Kolotouros, Georgios Pavlakos, Xiaowei Zhou, and Kostas Daniilidis. Coherent reconstruction of multiple humans from a single image. In *Proceedings of the IEEE/CVF Conference on Computer Vision and Pattern Recognition*, pages 5579–5588, 2020. 1, 2
- [39] Hanbyul Joo, Hao Liu, Lei Tan, Lin Gui, Bart Nabbe, Iain Matthews, Takeo Kanade, Shohei Nobuhara, and Yaser Sheikh. Panoptic studio: A massively multiview system for social motion capture. In *Proceedings of the IEEE International Conference on Computer Vision*, pages 3334–3342, 2015. 1
- [40] Hanbyul Joo, Tomas Simon, Xulong Li, Hao Liu, Lei Tan, Lin Gui, Sean Banerjee, Timothy Scott Godisart, Bart Nabbe, Iain Matthews, Takeo Kanade, Shohei Nobuhara, and Yaser Sheikh. Panoptic studio: A massively multiview system for social interaction capture. *IEEE Transactions on Pattern Analysis and Machine Intelligence*, 2017. 2, 5, 6, 7, 8, 9, 14, 15
- [41] Angjoo Kanazawa, Michael J Black, David W Jacobs, and Jitendra Malik. End-to-end recovery of human shape and pose. In *Proceedings of the IEEE conference on computer vision and pattern recognition*, pages 7122–7131, 2018. 1, 2
- [42] Petr Kellnhofer, Lars C Jebe, Andrew Jones, Ryan Spicer, Kari Pulli, and Gordon Wetzstein. Neural lumigraph rendering. In *Proceedings of the IEEE/CVF Conference on Computer Vision and Pattern Recognition*, pages 4287–4297, 2021. 2
- [43] Mijeong Kim, Seonguk Seo, and Bohyung Han. Infonerf: Ray entropy minimization for few-shot neural volume rendering. In *Proceedings of the IEEE/CVF Conference on Computer Vision and Pattern Recognition*, pages 12912–12921, 2022. 2, 5, 7
- [44] Diederik P Kingma and Jimmy Ba. Adam: A method for stochastic optimization. *arXiv preprint arXiv:1412.6980*, 2014. 5
- [45] Muhammed Kocabas, Nikos Athanasiou, and Michael J. Black. VIBE: Video inference for human body pose and shape estimation. In *2020 IEEE/CVF Conference on Computer Vision and Pattern Recognition (CVPR 2020)*, pages 5252–5262, Piscataway, NJ, June 2020. IEEE. 1, 2
- [46] Youngjoong Kwon, Dahun Kim, Duygu Ceylan, and Henry Fuchs. Neural human performer: Learning generalizable radiance fields for human performance rendering. *Advances in Neural Information Processing Systems*, 34, 2021. 1, 2
- [47] Vincent Leroy, Jean-Sébastien Franco, and Edmond Boyer. Shape reconstruction using volume sweeping and learned photoconsistency. In *Proceedings of the European Conference on Computer Vision (ECCV)*, pages 781–796, 2018. 2
- [48] Qian Li, Franck Multon, and Adnane Boukhayma. Learn-

- ing generalizable light field networks from few images. In *ICASSP 2023-2023 IEEE International Conference on Acoustics, Speech and Signal Processing (ICASSP)*, pages 1–5. IEEE, 2023. 2
- [49] Qian Li, Franck Multon, and Adnane Boukhayma. Regularizing neural radiance fields from sparse rgb-d inputs. In *2023 IEEE International Conference on Image Processing (ICIP)*, pages 2320–2324. IEEE, 2023. 2
- [50] Junbang Liang and Ming C Lin. Shape-aware human pose and shape reconstruction using multi-view images. In *Proceedings of the IEEE/CVF International Conference on Computer Vision*, pages 4352–4362, 2019. 2
- [51] Stefan Lionar, Daniil Emtsev, Dusan Svilarkovic, and Songyou Peng. Dynamic plane convolutional occupancy networks. In *Proceedings of the IEEE/CVF Winter Conference on Applications of Computer Vision*, pages 1829–1838, 2021. 2
- [52] Lingjie Liu, Marc Habermann, Viktor Rudnev, Kripasindhu Sarkar, Jiatao Gu, and Christian Theobalt. Neural actor: Neural free-view synthesis of human actors with pose control. *ACM Transactions on Graphics (TOG)*, 40(6):1–16, 2021. 1, 2
- [53] Wu Liu and Tao Mei. Recent advances of monocular 2d and 3d human pose estimation: A deep learning perspective. *ACM Computing Surveys (CSUR)*, 2022. 1, 2
- [54] Yebin Liu, Juergen Gall, Carsten Stoll, Qionghai Dai, Hans-Peter Seidel, and Christian Theobalt. Markerless motion capture of multiple characters using multiview image segmentation. *IEEE transactions on pattern analysis and machine intelligence*, 35(11):2720–2735, 2013. 2
- [55] Yebin Liu, Carsten Stoll, Juergen Gall, Hans-Peter Seidel, and Christian Theobalt. Markerless motion capture of interacting characters using multi-view image segmentation. In *CVPR 2011*, pages 1249–1256. Ieee, 2011. 1, 2
- [56] Xiaoxiao Long, Cheng Lin, Peng Wang, Taku Komura, and Wenping Wang. SparseNeuS: Fast generalizable neural surface reconstruction from sparse views. *ECCV*, 2022. 2, 3
- [57] Matthew Loper, Naureen Mahmood, Javier Romero, Gerard Pons-Moll, and Michael J Black. Smpl: A skinned multi-person linear model. *ACM transactions on graphics (TOG)*, 34(6):1–16, 2015. 1, 2
- [58] Ricardo Martin-Brualla, Noha Radwan, Mehdi SM Sajjadi, Jonathan T Barron, Alexey Dosovitskiy, and Daniel Duckworth. Nerf in the wild: Neural radiance fields for unconstrained photo collections. In *Proceedings of the IEEE/CVF Conference on Computer Vision and Pattern Recognition*, pages 7210–7219, 2021. 5
- [59] Ben Mildenhall, Pratul P Srinivasan, Matthew Tancik, Jonathan T Barron, Ravi Ramamoorthi, and Ren Ng. Nerf: Representing scenes as neural radiance fields for view synthesis. In *European conference on computer vision*, pages 405–421. Springer, 2020. 1, 2, 3, 4, 5, 14, 16
- [60] Lea Muller, Ahmed AA Osman, Siyu Tang, Chun-Hao P Huang, and Michael J Black. On self-contact and human pose. In *Proceedings of the IEEE/CVF Conference on Computer Vision and Pattern Recognition*, pages 9990–9999, 2021. 2
- [61] Armin Mustafa, Akin Caliskan, Lourdes Agapito, and Adrian Hilton. Multi-person implicit reconstruction from a single image. In *Proceedings of the IEEE/CVF Conference on Computer Vision and Pattern Recognition*, pages 14474–14483, 2021. 1, 2
- [62] Michael Niemeyer, Jonathan T Barron, Ben Mildenhall, Mehdi SM Sajjadi, Andreas Geiger, and Noha Radwan. Regnerf: Regularizing neural radiance fields for view synthesis from sparse inputs. In *Proceedings of the IEEE/CVF Conference on Computer Vision and Pattern Recognition*, pages 5480–5490, 2022. 2, 3
- [63] Michael Niemeyer, Lars Mescheder, Michael Oechsle, and Andreas Geiger. Differentiable volumetric rendering: Learning implicit 3d representations without 3d supervision. In *Proceedings of the IEEE/CVF Conference on Computer Vision and Pattern Recognition*, pages 3504–3515, 2020. 2
- [64] Michael Oechsle, Songyou Peng, and Andreas Geiger. Unisurf: Unifying neural implicit surfaces and radiance fields for multi-view reconstruction. In *Proceedings of the IEEE/CVF International Conference on Computer Vision*, pages 5589–5599, 2021. 2
- [65] Amine Ouasfi and Adnane Boukhayma. Few’zero level set’-shot learning of shape signed distance functions in feature space. In *ECCV*, 2022. 2
- [66] Amine Ouasfi and Adnane Boukhayma. Few-shot unsupervised implicit neural shape representation learning with spatial adversaries. *arXiv preprint arXiv:2408.15114*, 2024. 2
- [67] Amine Ouasfi and Adnane Boukhayma. Mixing-denoising generalizable occupancy networks. *3DV*, 2024. 2
- [68] Amine Ouasfi and Adnane Boukhayma. Robustifying generalizable implicit shape networks with a tunable non-parametric model. *Advances in Neural Information Processing Systems*, 36, 2024. 2
- [69] Amine Ouasfi and Adnane Boukhayma. Unsupervised occupancy learning from sparse point cloud. In *Proceedings of the IEEE/CVF Conference on Computer Vision and Pattern Recognition*, pages 21729–21739, 2024. 2
- [70] Amine Ouasfi, Shubhendu Jena, Eric Marchand, and Adnane Boukhayma. Toward robust neural reconstruction from sparse point sets, 2024. 2
- [71] Jeong Joon Park, Peter Florence, Julian Straub, Richard Newcombe, and Steven Lovegrove. Deepsdf: Learning continuous signed distance functions for shape representation. In *Proceedings of the IEEE/CVF conference on computer vision and pattern recognition*, pages 165–174, 2019. 1, 3
- [72] Adam Paszke, Sam Gross, Francisco Massa, Adam Lerer, James Bradbury, Gregory Chanan, Trevor Killeen, Zeming Lin, Natalia Gimelshein, Luca Antiga, et al. Pytorch: An imperative style, high-performance deep learning library. *Advances in neural information processing systems*, 32, 2019. 5
- [73] Sida Peng, Junting Dong, Qianqian Wang, Shangzhan Zhang, Qing Shuai, Xiaowei Zhou, and Hujun Bao. Animatable neural radiance fields for modeling dynamic human bodies. In *Proceedings of the IEEE/CVF International Conference on Computer Vision*, pages 14314–14323, 2021. 1, 2
- [74] Songyou Peng, Chiyu Jiang, Yiyi Liao, Michael Niemeyer,

- Marc Pollefeys, and Andreas Geiger. Shape as points: A differentiable poisson solver. *Advances in Neural Information Processing Systems*, 34:13032–13044, 2021. 2
- [75] Songyou Peng, Michael Niemeyer, Lars Mescheder, Marc Pollefeys, and Andreas Geiger. Convolutional occupancy networks. In *European Conference on Computer Vision*, pages 523–540. Springer, 2020. 2
- [76] Sida Peng, Yuanqing Zhang, Yinghao Xu, Qianqian Wang, Qing Shuai, Hujun Bao, and Xiaowei Zhou. Neural body: Implicit neural representations with structured latent codes for novel view synthesis of dynamic humans. In *Proceedings of the IEEE/CVF Conference on Computer Vision and Pattern Recognition*, pages 9054–9063, 2021. 1, 2
- [77] Barbara Roessle, Jonathan T Barron, Ben Mildenhall, Pratul P Srinivasan, and Matthias Nießner. Dense depth priors for neural radiance fields from sparse input views. In *Proceedings of the IEEE/CVF Conference on Computer Vision and Pattern Recognition*, pages 12892–12901, 2022. 2, 3
- [78] Shunsuke Saito, Zeng Huang, Ryota Natsume, Shigeo Morishima, Angjoo Kanazawa, and Hao Li. Pifu: Pixel-aligned implicit function for high-resolution clothed human digitization. In *Proceedings of the IEEE/CVF International Conference on Computer Vision*, pages 2304–2314, 2019. 2
- [79] Shunsuke Saito, Tomas Simon, Jason Saragih, and Hanbyul Joo. Pifuhd: Multi-level pixel-aligned implicit function for high-resolution 3d human digitization. In *Proceedings of the IEEE/CVF Conference on Computer Vision and Pattern Recognition*, pages 84–93, 2020. 2
- [80] Qing Shuai, Chen Geng, Qi Fang, Sida Peng, Wenhao Shen, Xiaowei Zhou, and Hujun Bao. Novel view synthesis of human interactions from sparse multi-view videos. In *ACM SIGGRAPH 2022 Conference Proceedings*, pages 1–10, 2022. 2
- [81] Tomas Simon, Hanbyul Joo, and Yaser Sheikh. Hand key-point detection in single images using multiview bootstrapping. *CVPR*, 2017. 2, 5, 6, 7, 8, 9, 14, 15
- [82] Jonathan Starck and Adrian Hilton. Surface capture for performance-based animation. *IEEE computer graphics and applications*, 27(3):21–31, 2007. 2
- [83] Yu Sun, Qian Bao, Wu Liu, Yili Fu, Michael J Black, and Tao Mei. Monocular, one-stage, regression of multiple 3d people. In *Proceedings of the IEEE/CVF International Conference on Computer Vision*, pages 11179–11188, 2021. 1, 2
- [84] Yu Sun, Wu Liu, Qian Bao, Yili Fu, Tao Mei, and Michael J Black. Putting people in their place: Monocular regression of 3d people in depth. In *Proceedings of the IEEE/CVF Conference on Computer Vision and Pattern Recognition*, pages 13243–13252, 2022. 1, 2
- [85] Matthew Tancik, Pratul Srinivasan, Ben Mildenhall, Sara Fridovich-Keil, Nithin Raghavan, Utkarsh Singhal, Ravi Ramamoorthi, Jonathan Barron, and Ren Ng. Fourier features let networks learn high frequency functions in low dimensional domains. *Advances in Neural Information Processing Systems*, 33:7537–7547, 2020. 4, 16
- [86] Justus Thies, Michael Zollhöfer, and Matthias Nießner. Deferred neural rendering: Image synthesis using neural textures. *Acm Transactions on Graphics (TOG)*, 38(4):1–12, 2019. 2
- [87] Nicolas Ugrinovic, Adria Ruiz, Antonio Agudo, Alberto Sanfeliu, and Francesc Moreno-Noguer. Body size and depth disambiguation in multi-person reconstruction from single images. In *2021 International Conference on 3D Vision (3DV)*, pages 53–63. IEEE, 2021. 1, 2
- [88] Daniel Vlasic, Ilya Baran, Wojciech Matusik, and Jovan Popović. Articulated mesh animation from multi-view silhouettes. In *ACM SIGGRAPH 2008 papers*, pages 1–9. 2008. 2
- [89] Daniel Vlasic, Pieter Peers, Ilya Baran, Paul Debevec, Jovan Popović, Szymon Rusinkiewicz, and Wojciech Matusik. Dynamic shape capture using multi-view photometric stereo. In *ACM SIGGRAPH Asia 2009 papers*, pages 1–11. 2009. 1, 2
- [90] Peng Wang, Lingjie Liu, Yuan Liu, Christian Theobalt, Taku Komura, and Wenping Wang. Neus: Learning neural implicit surfaces by volume rendering for multi-view reconstruction. *arXiv preprint arXiv:2106.10689*, 2021. 1, 2, 3, 5, 6, 8, 14, 15
- [91] Shaofei Wang, Katja Schwarz, Andreas Geiger, and Siyu Tang. Arah: Animatable volume rendering of articulated human sdf. In *European Conference on Computer Vision*, 2022. 1, 2, 5, 7, 14, 16
- [92] Zhou Wang, Alan C Bovik, Hamid R Sheikh, and Eero P Simoncelli. Image quality assessment: from error visibility to structural similarity. *IEEE transactions on image processing*, 13(4):600–612, 2004. 5
- [93] Chung-Yi Weng, Brian Curless, Pratul P Srinivasan, Jonathan T Barron, and Ira Kemelmacher-Shlizerman. Humannerf: Free-viewpoint rendering of moving people from monocular video. In *Proceedings of the IEEE/CVF Conference on Computer Vision and Pattern Recognition*, pages 16210–16220, 2022. 1, 2
- [94] Francis Williams, Zan Gojcic, Sameh Khamis, Denis Zorin, Joan Bruna, Sanja Fidler, and Or Litany. Neural fields as learnable kernels for 3d reconstruction. In *CVPR*, 2022. 2
- [95] Francis Williams, Matthew Trager, Joan Bruna, and Denis Zorin. Neural splines: Fitting 3d surfaces with infinitely-wide neural networks. In *CVPR*, 2021. 2
- [96] Chenglei Wu, Carsten Stoll, Levi Valgaerts, and Christian Theobalt. On-set performance capture of multiple actors with a stereo camera. *ACM Transactions on Graphics (TOG)*, 32(6):1–11, 2013. 1, 2
- [97] Chenglei Wu, Kiran Varanasi, and Christian Theobalt. Full body performance capture under uncontrolled and varying illumination: A shading-based approach. In *European Conference on Computer Vision*, pages 757–770. Springer, 2012. 2
- [98] Minye Wu, Yuehao Wang, Qiang Hu, and Jingyi Yu. Multi-view neural human rendering. In *Proceedings of the IEEE/CVF Conference on Computer Vision and Pattern Recognition*, pages 1682–1691, 2020. 2
- [99] Hongyi Xu, Thiemo Alldieck, and Cristian Sminchisescu. H-nerf: Neural radiance fields for rendering and temporal reconstruction of humans in motion. *Advances in Neural Information Processing Systems*, 34:14955–14966, 2021. 1, 2
- [100] Lior Yariv, Jiatao Gu, Yoni Kasten, and Yaron Lipman.

- Volume rendering of neural implicit surfaces. *Advances in Neural Information Processing Systems*, 34:4805–4815, 2021. [1](#), [2](#), [5](#), [6](#), [8](#), [14](#), [15](#)
- [101] Lior Yariv, Yoni Kasten, Dror Moran, Meirav Galun, Matan Atzmon, Basri Ronen, and Yaron Lipman. Multiview neural surface reconstruction by disentangling geometry and appearance. *Advances in Neural Information Processing Systems*, 33:2492–2502, 2020. [1](#), [2](#), [3](#), [4](#), [5](#)
- [102] Mae Younes, Amine Ouasfi, and Adnane Boukhayma. Sparsecraft: Few-shot neural reconstruction through stereopsis guided geometric linearization. In *European Conference on Computer Vision*, pages 37–56. Springer, 2025. [2](#)
- [103] Alex Yu, Vickie Ye, Matthew Tancik, and Angjoo Kanazawa. pixelnerf: Neural radiance fields from one or few images. In *Proceedings of the IEEE/CVF Conference on Computer Vision and Pattern Recognition*, pages 4578–4587, 2021. [2](#)
- [104] Tao Yu, Kaiwen Guo, Feng Xu, Yuan Dong, Zhaoqi Su, Jianhui Zhao, Jianguo Li, Qionghai Dai, and Yebin Liu. Bodyfusion: Real-time capture of human motion and surface geometry using a single depth camera. In *Proceedings of the IEEE International Conference on Computer Vision*, pages 910–919, 2017. [1](#), [2](#)
- [105] Tao Yu, Zerong Zheng, Kaiwen Guo, Pengpeng Liu, Qionghai Dai, and Yebin Liu. Function4d: Real-time human volumetric capture from very sparse consumer rgbd sensors. In *IEEE Conference on Computer Vision and Pattern Recognition (CVPR2021)*, June 2021. [7](#), [16](#)
- [106] Tao Yu, Zerong Zheng, Kaiwen Guo, Jianhui Zhao, Qionghai Dai, Hao Li, Gerard Pons-Moll, and Yebin Liu. Doublefusion: Real-time capture of human performances with inner body shapes from a single depth sensor. In *Proceedings of the IEEE conference on computer vision and pattern recognition*, pages 7287–7296, 2018. [1](#), [2](#)
- [107] Ye Yuan, Umar Iqbal, Pavlo Molchanov, Kris Kitani, and Jan Kautz. Glamr: Global occlusion-aware human mesh recovery with dynamic cameras. In *Proceedings of the IEEE/CVF Conference on Computer Vision and Pattern Recognition (CVPR)*, 2022. [2](#)
- [108] Andrei Zanfir, Elisabeta Marinoiu, and Cristian Sminchisescu. Monocular 3d pose and shape estimation of multiple people in natural scenes-the importance of multiple scene constraints. In *Proceedings of the IEEE Conference on Computer Vision and Pattern Recognition*, pages 2148–2157, 2018. [1](#), [2](#)
- [109] Andrei Zanfir, Elisabeta Marinoiu, Mihai Zanfir, Alin-Ionut Popa, and Cristian Sminchisescu. Deep network for the integrated 3d sensing of multiple people in natural images. *Advances in Neural Information Processing Systems*, 31, 2018. [1](#), [2](#)
- [110] Jiakai Zhang, Xinhang Liu, Xinyi Ye, Fuqiang Zhao, Yanshun Zhang, Minye Wu, Yingliang Zhang, Lan Xu, and Jingyi Yu. Editable free-viewpoint video using a layered neural representation. *ACM Transactions on Graphics (TOG)*, 40(4):1–18, 2021. [1](#)
- [111] Jianfeng Zhang, Dongdong Yu, Jun Hao Liew, Xuecheng Nie, and Jiashi Feng. Body meshes as points. In *Proceedings of the IEEE/CVF Conference on Computer Vision and Pattern Recognition*, pages 546–556, 2021. [1](#), [2](#)
- [112] Jason Y Zhang, Sam Ppose, Hanbyul Joo, Deva Ramanan, Jitendra Malik, and Angjoo Kanazawa. Perceiving 3d human-object spatial arrangements from a single image in the wild. In *European conference on computer vision*, pages 34–51. Springer, 2020. [2](#)
- [113] Kai Zhang, Gernot Riegler, Noah Snavely, and Vladlen Koltun. Nerf++: Analyzing and improving neural radiance fields. *arXiv preprint arXiv:2010.07492*, 2020. [3](#)
- [114] Richard Zhang, Phillip Isola, Alexei A Efros, Eli Shechtman, and Oliver Wang. The unreasonable effectiveness of deep features as a perceptual metric. In *Proceedings of the IEEE conference on computer vision and pattern recognition*, pages 586–595, 2018. [5](#)
- [115] Yuxiang Zhang, Zhe Li, Liang An, Mengcheng Li, Tao Yu, and Yebin Liu. Lightweight multi-person total motion capture using sparse multi-view cameras. In *Proceedings of the IEEE/CVF International Conference on Computer Vision*, pages 5560–5569, 2021. [1](#), [2](#)
- [116] Yang Zheng, Ruizhi Shao, Yuxiang Zhang, Tao Yu, Zerong Zheng, Qionghai Dai, and Yebin Liu. Deepmulticap: Performance capture of multiple characters using sparse multiview cameras. In *Proceedings of the IEEE/CVF International Conference on Computer Vision*, pages 6239–6249, 2021. [1](#), [2](#), [7](#), [8](#), [9](#), [16](#)

Few-Shot Multi-Human Neural Rendering Using Geometry Constraints

Supplementary Material

6. Additional Results

Scene editing. We show here how our method can be used to perform post-learning scene editing without any additional training. Thanks to the human bounding-box-based modeling of the foreground scene, it is straightforward to rigidly transform or omit each person by simply applying, before rendering, the corresponding manipulation to the points sampled inside the defined bounding box. Figure 7 shows qualitative results of such application, trained on scene #5 from the CMU Panoptic dataset [40, 81] using 20 training views. We can see here that our approach can generate realistic new scenes as well as plausible inpaintings of the missing regions.

Comparisons with varying number of people. In Fig. 8 we provide additional qualitative comparisons against NeuS [90] and VolSDF [100], where we show results on the CMU Panoptic dataset [40, 81] with varying number of people in the scene (Going from 3 to 7 people). Note here how increasing the number of people reduces the quality of our baselines results, *i.e.* mixing the background with humans or generating noisy geometries. Meanwhile, our method performs consistently, independently of the number of people.

Additional Quantitative Results. Table 5 provides a full Chamfer distance comparison in the synthetic data setup as an addition to the results reported in Table 3 of the main submission. Symbol ‘-’ represents cases where the baselines fail to reconstruct a meaningful geometry, and hence the error is too large. To favor the baselines NeuS [90] and VolSDF [100] in the main submission, we computed the uni-directional Chamfer distance from ground-truth to source, as the baselines reconstructed the ground of the scene in addition to the people. For a more standard evaluation, we additionally show here the bi-directional Chamfer distance after removing the floor for the competing methods.

Comparison to single human NeRF In Figure 4 in the main submission, we compared our work to the single human NeRF method ARAH [91] on the CMU Panoptic dataset [40, 81]. Figure 9 shows the training images used in this experiment. It also shows the segmentation masks used for ARAH for 3 people in the scene, that we built using a state-of-the-art method. Figure 9 shows additional comparative results for reconstructed appearance and geometry.

# People	Method	one-way Chamfer ↓			bidirectional Chamfer ↓		
		5	10	15	5	10	15
1	NeuS	-	-	0.308	-	-	3.026
	VolSDF	-	0.020	0.019	-	0.039	0.167
	Ours	0.025	0.019	0.018	0.271	0.211	0.154
5	NeuS	-	-	0.321	-	-	3.044
	VolSDF	-	-	0.151	-	-	1.478
	Ours	0.025	0.023	0.020	0.391	0.289	0.138
10	NeuS	-	-	0.383	-	-	4.639
	VolSDF	-	-	0.248	-	-	1.579
	Ours	0.082	0.063	0.043	0.111	0.085	0.081

Table 5. Geometry reconstruction error under varying number of people, compared to NeuS [90] and VolSDF [100] using the synthetic dataset, with 5/10/15 views for training. Symbol ‘-’ represents cases where the baselines fail to reconstruct a meaningful geometry.

7. Implementation Details

Fig. 11 shows the architecture of our network in more detail (Section 3 in the main submission). The geometry MLP has 8 layers of width 256, with a skip connection from the input to the 4th layer. The radiance MLP consists of additional 4 layers of width 256, and receives as input the positional encoding of the point $\gamma(p)$, positional encoding of the view direction $\gamma(v)$, rasterized depth feature f_1 , and gradient of the SDF $n(p)$. All layers are linear with ReLU activation, except for the last layer which uses a sigmoid activation function. During training we sample 512 rays per batch and follow the coarse and fine sampling strategy of [59, 90]. For a fair comparison, we unified the number of sampled points on each ray for all methods, namely, each ray with $N = 64$ coarsely sampled points and $N = 64$ finely sampled points for the foreground, and $N = 32$ for the background.

Fig. 12 illustrates the losses involved in the training of our method. Rays with available ground-truth pixels are supervised with pixel colors. Sub-pixel rays without available ground-truth are supervised using color and density pseudo-ground-truth from neighboring rays.

8. Datasets

We provide here additional details on the evaluation datasets used in Section 4 from the main paper.

CMU Panoptic [40, 81]. Our experiments were performed on five different scenes from the CMU Panoptic dataset [40, 81], where each scene includes originally 30 views located on a spherical spiral. The training views

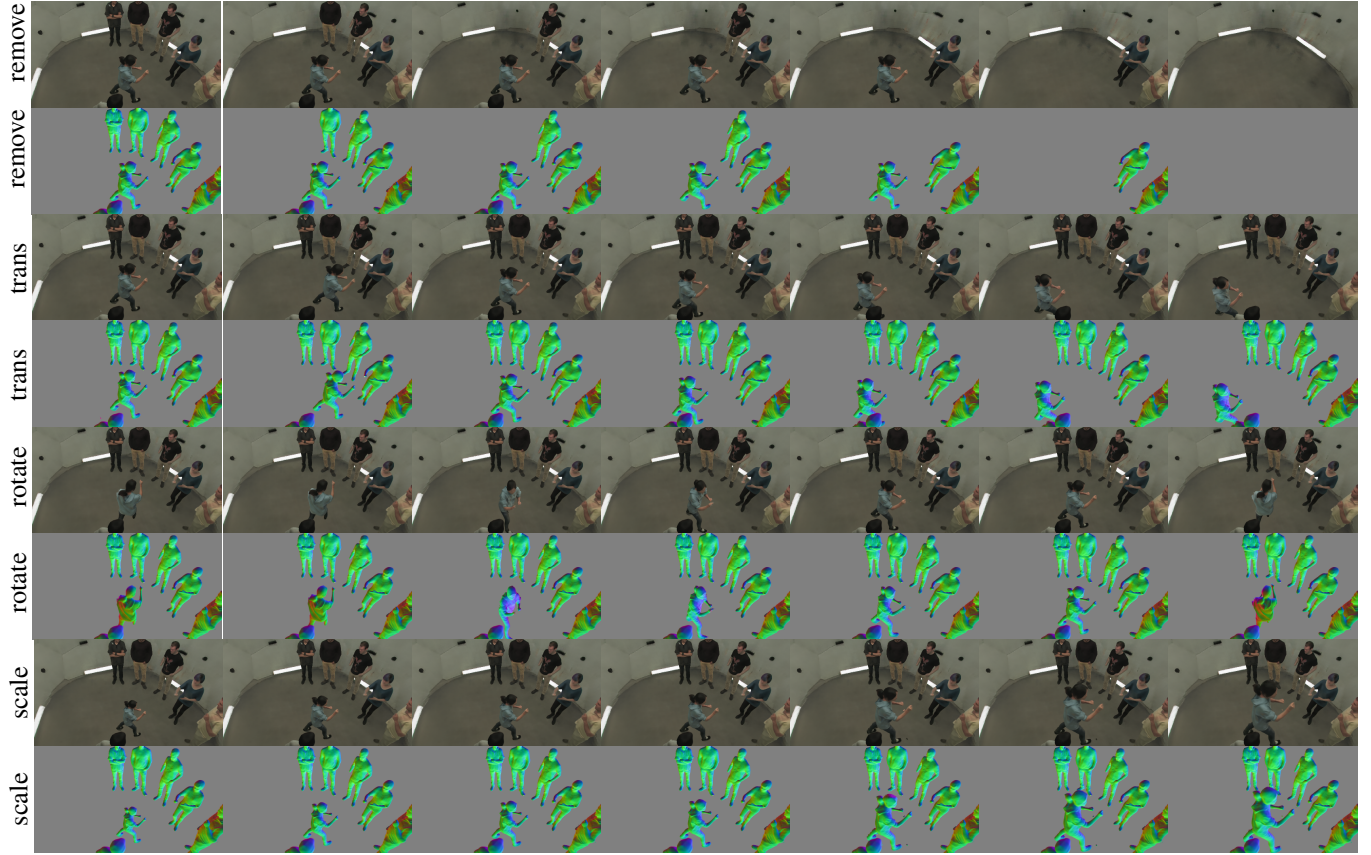


Figure 7. Qualitative results for the editing application. We show synthesised novel views and reconstructed normal images of multiple humans when (1) removing, (2) translating, (3) rotating and (4) scaling subjects in the scene.

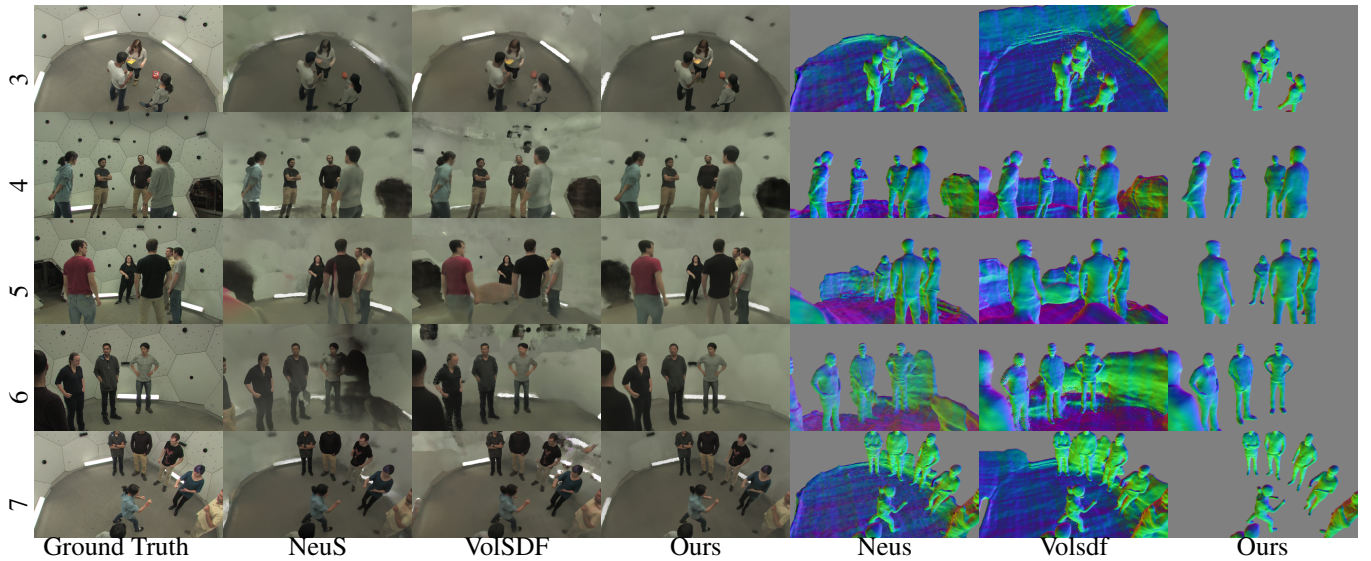


Figure 8. Qualitative comparisons against NeuS [90] and VoISDF [100] for different number of people in the scene. Showing synthesised novel views and reconstructed normal images on 5 scenes from CMU Panoptic dataset [40, 81], using 20 training views.



Figure 9. The five training views and person segmentations used to produce results in Figure 4 of the main submission.

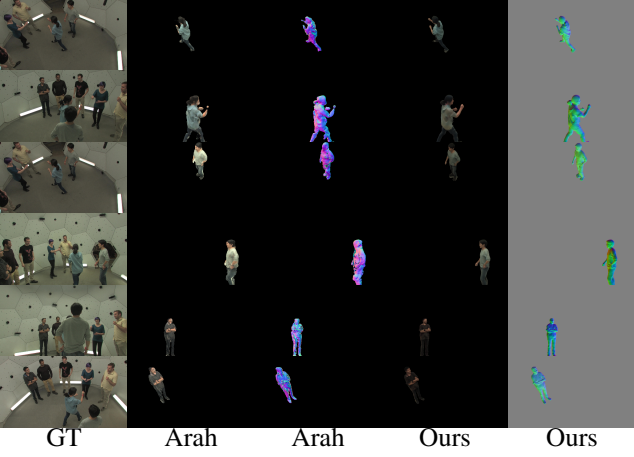


Figure 10. Comparison against single human method ARAH [91] using 5 training views. The average PSNR in these examples is 24.11/27.40 (ARAH/Ours).

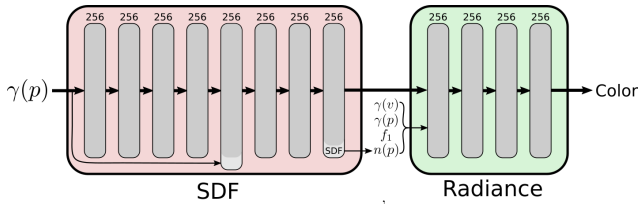


Figure 11. **Network architecture** (Section 3 of the main submission). p is a sampled point along a ray. γ is the positional encoding [59, 85]. $n(p)$ is the gradient of predicted sdf w.r.t the input point p . v is the direction of the ray, and f_1 the rasterized depth feature described in Section 3.2.

were randomly extracted from the HD sequences ‘Ultimatum’ and ‘Haggling’, and contain between 3 and 7 people. Specifically, we used frame 9200 from ‘Haggling’, and frames 5500, 7800, 9200 and 22900 from ‘Ultimatum’. We uniformly sampled 5, 10, 15 and 20 views as training and we used the remaining 25, 20, 15 and 10 views respectively as testing. The image resolution in training and testing is 1920×1080 .

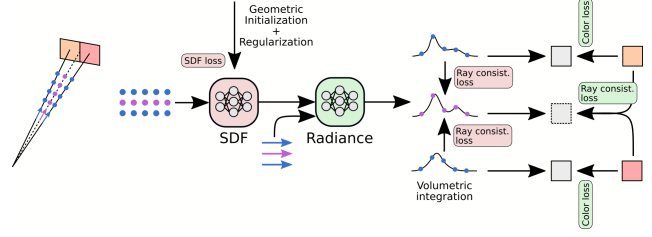


Figure 12. Illustration of our losses. Rays without ground-truth are supervised using our ray consistency loss (Section 3.4). For rays corresponding to pixels in the training data, we supervise points using a combination of SDF losses and color losses (Section 3.4).

Synthetic Dataset from MultiHuman-Dataset [105, 116]

Based on the MultiHuman-Dataset [105, 116], we rendered a synthetic dataset with 29 cameras arranged in a sphere. There are three scenes in this dataset with similar backgrounds but different lighting conditions, camera locations and orientations. The scenes contain 1, 5 and 10 people respectively. The image resolution is 1920×1080 . We sample 5, 10 and 15 views uniformly on each scene for training, and 14 views for testing.